International Journal of Research
Available at https://edupediapublications.org/journals
p-ISSN: 2348-6848
e-ISSN: 2348-795X
Volume 02 Issue 11
November 2015

Co-Ordination of Solar and Wind Power for A Dc Micro Grid

Mr. B.Rajendra Prasad Tenali
Assistant Professor, Department of Electrical And Electronics, B.V.C College of Engineering, Rajahmundry,A.P., India

Abstract—
This work presents a performance study of a dc microgrid with the integration of wind and solar power when it is used a voltage droop technique to regulated the grid voltage and to control the load sharing between different sources. Compared with the existing droop controls, it is distinguished in that the droop curves are set as a function of the storage state-of-charge (SOC) and can become asymmetric. The adaptation of the slopes ensures that the power output supports the terminal voltage while at the same keeping the SOC within a target range of desired operational reserve. This is shown to maintain the equilibrium of the microgrid's real-time supply and demand. A small model of a dc microgrid comprising micro sources and loads was implemented in the Simulink/Matlab environment.

Index Terms- Distributed energy resources; droop control; electric vehicle (EV); emission constraint, fast charging; microgrid; multilevel energy storage

I. INTRODUCTION

IN the year 2012, 44.8 GW of new wind energy conversion systems were installed worldwide [1]. The trend has been toward increasingly larger turbine sizes, culminating in the installation of off-shore wind parks that are located far from the load centers [2]. This can lead to rather large distances between generation and load in the electricity sector. The transportation sector reveals an even larger disconnect between the locations of fuel production and consumption. The energy system proposed in this paper seeks to address both issues related to electricity and transportation sectors. One potential solution is a microgrid that can be vertically integrated with a high-rise building as frequently encountered in urban areas. The harvesting of renewable wind and solar energy occurs at the top of the building. The rooftop generation connects to the ground level via a microgrid where electric vehicle (EV) charging stations are supplied, and a battery supports maintaining the balance of supply and demand. The potential value of an urban integration within buildings as considered here comes from the usage of rooftop energy resources, the storage of the latter for offering EV fast charging at the ground level, the contribution to emission-free EV transportation in urban areas, the co-location and integration of generation and load in urban areas, and the grid-friendly integration of the microgrid with the rest of the power system main grid. The combination of wind and solar energy resources on a rooftop was also investigated in [3]. It was verified that the combination of wind and solar energy leads to reduced local storage requirements [4]. The combination of diverse but complementary storage technologies in turn can form a multilevel energy storage, where a super capacitor or flywheel provides cache control to compensate for fast power fluctuations and to smoothen the transients encountered by a battery with higher energy capacity [5], [6]. Microgrids or hybrid energy systems have been shown to be an effective structure for local interconnection of distributed renewable generation, loads, and storage [7]–[12]. Recent research has considered the optimization of the operation on one hand [13]–[15] and the usage of dc to link the resources on the other [16]–[18]. The dc link voltage was shown to be maintained by a droop control that relates the dc link voltage to the power output of

International Journal of Research
Available at https://edupediapublications.org/journals
p-ISSN: 2348-6848
e-ISSN: 2348-795X
Volume 02 Issue 11
November 2015

controllable resources. In this paper, it is proposed to set the droop as a function of the expected state of charge (SOC) of the battery according to its operational optimization set point versus the actual realtime SOC. The proposed operational optimization is further distinguished in that it quantifies the uncertainty associated with renewable generation forecast, emission constraints, and EV fast charging. Following this introduction, an outline of the principle of a dc microgrid is given in Section II. In Section III, a method is developed for quantifying the aggregated wind and solar power forecast uncertainty, the resulting required SOC of the battery, and the operational optimization. The optimization-guided droop control is dealt with in Section IV. A case study involving a time series

and

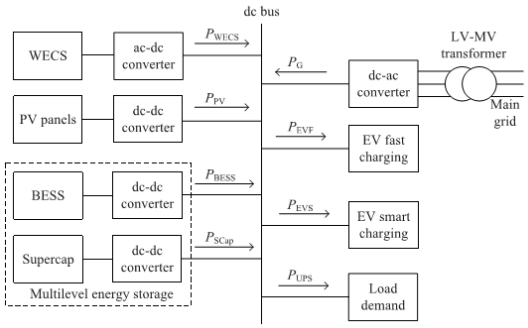

Figure 1 layout of dc micro grid

Fig.2 wind and PV based power generation for the verticallyintegratedmicrogrid

simulation over diverse time scales to substantiate the claims made is discussed in Section V. Conclusions are drawn in Section VI.

II. OUTLINE OFDC MICROGRID

A schematic of the dc microgrid with the conventions employed for power is given in Fig. 1. The dc bus connects wind energy conversion system (WECS), PV panels, multilevel energy storage comprising battery energy storage system (BESS) and supercapacitor, EV smart charging points, EV fast charging station, and grid interface. The WECS is connected to the dc bus via an ac–dc converter. PV panels are connected to the dc bus via a dc–dc converter. The BESS can be realized through flow battery technology connected to the dc bus via a dc–dc converter. The supercapacitor has much less energy capacity than the BESS. Rather, it is aimed at compensating for fast fluctuations of power and so provides cache control as detailed in [19].

Thanks to the multilevel energy storage, the intermittent and volatile renewable power outputs can be managed, and a deterministic controlled power to the main grid is obtained by optimization. Providing uninterruptible power supply (UPS)

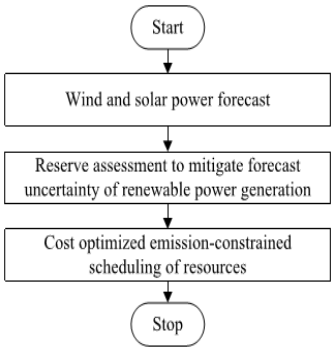

Figure 2 overview of optimized scheduling approach

service to loads when needed is a core duty of the urban microgrid. EV fast charging introduces a stochastic load to the microgrid. The multilevel energy storage mitigates potential impacts on the main grid. In building integration, a vertical axis wind turbine may be installed on the rooftop as shown in Fig. 2. PV panels can be co-located on the rooftop andthe facade of the building. Such or similar configurations benefit from a local availability of abundant wind and solar energy. The fast charging station is realized for public

International Journal of Research
Available at https://edupediapublications.org/journals
p-ISSN: 2348-6848
e-ISSN: 2348-795X
Volume 02 Issue 11
November 2015

access at the ground level. It is connected close to the LV–MV transformer to reduce losses and voltage drop. EVs parked in the building are offered smart charging within user-defined constraints.

III. OPERATIONALOPTIMIZATI ON OFMICROGRID

FORRENEWABLEENERGYINTEGRATION

The algorithm for optimized scheduling of the microgrid is depicted in Fig. 3. In the first stage, wind and solar power generation are forecast.The uncertainty of the wind and solar power is presented by a three-state model. An example of such a forecast is shown in Fig. 4. State 1 represents a power forecast lower than the average power forecast. This state is shown by the power forecast of P1with the forecast probability of pr1 assigned to it. The average power forecast and the probability of forecast assigned to it give state 2. State 3 represents a power forecast higher than the average power forecast. Then, wind and solar power forecasts are aggregated to produce the total renewable power forecast model. This aggregation method is formulated in Section III-A. The aggregated power generation data are used to assign hourly positive and negative energy reserves to the BESS for the microgrid operation. The positive energy reserve of the BESS gives the energy stored that can be readily injected into the dc bus on demand. The negative energy reserve gives the part of the BESS to remain uncharged to capture excess power on demand. Energy reserve assessment is performed according to the aggregated renewable power generation forecast. In order to compensate for the uncertainty of the forecast, a method is devised to assess positive and negative energy reserves in Section III-B. Finally, the emissionconstrained cost optimization is formulated to schedule the microgrid resources for the day-ahead dispatch. The optimized scheduling is formulated in Section III-C.

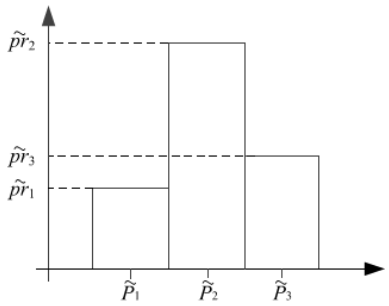

Figure 3 wind or solar power forecast uncertainty for 1h.

TABLE I
EXAMPLE A: WIND AND SOLAR POWER FORECAST DATA

Individual state	State 1	State 2	State 3
Wind forecast probability	0.25	0.50	0.25
Wind power (kW)	40	50	60
Solar forecast probability	0.25	0.50	0.25
Solar power (kW)	15	20	25

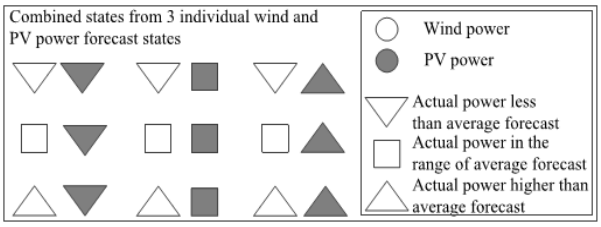

Figure 4 Aggregation of wind and solar power forecast in microgrid

A. Aggregated Model of Wind and Solar Power Forecast

Wind and solar power generation forecast uncertainty data are made available for the urban microgrid. Specifically, as shown in Fig. 4, the output power state and the probability assigned to that state are available. In the three-state model, the number of individual states is K=3. A sample of forecast data of the wind and solar power generation is provided for 1 h, as shown in Table I. For example, at a probability of 50% the wind power will be 50 kW in state 2. The aggregation of output power states of the wind and solar power is formed as follows. As the microgrid has two generation resources with three individual states, K =3, the number of combined states is N=K2 , which is equal to nine in this case. The combined

International Journal of Research
Available at https://edupediapublications.org/journals
p-ISSN: 2348-6848
e-ISSN: 2348-795X
Volume 02 Issue 11
November 2015

states in the forecast uncertainty model of wind and solar power are shown in Fig. 5. In each combined state, the power of those individual states is summed up, and the probability of a combined state is the product of the probabilities in individual states assuming that the individual states are not correlated. For the wind and PV power forecast shown in Table I, nine combined states are defined. Those states are provided in Table II. The combined states, as shown by the example in Table II, should be reduced to fewer representative states. To aggregate the combined states, Maggregated states are defined. In this exampleM=3. Those states are shown in Table II and denoted bym. The borders between aggregated

TABLE II
EXAMPLE A: COMBINED STATES OF WIND AND SOLAR POWER FORECAST

Combined state n	Counter l	Aggregated state m	Power output $\widetilde{P}_{l,m}$ (kW)	Probability $\widetilde{pr}_{l,m}$
1	1	1	40 + 15 = 55	0.25 × 0.25 = 0.0625
2	2	1	40 + 20 = 60	0.25 × 0.50 = 0.1250
3	1	2	40 + 25 = 65	0.25 × 0.25 = 0.0625
4	2	2	50 + 15 = 65	0.50 × 0.25 = 0.1250
5	3	2	50 + 20 = 70	0.50 × 0.50 = 0.2500
6	4	2	50 + 25 = 75	0.50 × 0.25 = 0.1250
7	5	2	60 + 15 = 75	0.25 × 0.25 = 0.0625
8	1	3	60 + 20 = 80	0.25 × 0.50 = 0.1250
9	2	3	60 + 25 = 85	0.25 × 0.25 = 0.0625

states are determined based on the borders between individual states in Table I. The average renewable power of individual states 1 and 2 is 62.5 kW and gives the border between aggregated states 1 and 2. Likewise, the average renewable power of individual states 2 and 3 gives the border between aggregated states 2 and 3. If an aggregated state mcovers a number of combined states L, the probability of having one of those aggregated states is the sum of the probabilities of those combined states

$$\widetilde{pr}_{A,m} = \sum_{l=1}^{L} \widetilde{pr}_{l,m} \qquad (1)$$

Where prA,mis the forecast probability of renewable power at the aggregated statem,and prl,mis the forecast probability of renewable power at the combined statel within the aggregated state m. The average power of each aggregated state is calculated by the average weighting of all power outputs in the aggregated state m

$$\widetilde{P}_{A,m} = \frac{\sum_{l=1}^{L} \widetilde{pr}_{l,m} \times \widetilde{P}_{l,m}}{\widetilde{pr}_{A,m}} \qquad (2)$$

where PA,mis the power forecast of renewables at the aggregated statem,and Pl,mis the power forecast at the combined statel within the aggregated statement. In the example shown in Table II, the combined model is reduced to a three-state wind and solar power forecast model. Employing (1) and (2), the calculation is shown for aggregated state 1 in the following:

$$\widetilde{pr}_{A,1} = 0.0625 + 0.1250 = 0.1875$$
$$\widetilde{P}_{A,1} = \frac{55 \times 0.0625 + 60 \times 0.1250}{0.1875}\,\text{kW} = 58.33\ \text{kW}.$$

A summary of the aggregated three-state model for the renewable power generation is provided in Table III. In this table, the power output at state 2 represents the average renewable energy source power forecast and is used for optimized scheduling. This three-state model is chosen as an illustrative example because it is the minimum model to represent power generation forecast uncertainty. More states may be used if deemed appropriate. The aggregated output power states are employed to calculate required hourly positive and negative energy reserves in

TABLE III
EXAMPLE A: SINGLE HOUR OF AGGREGATED THREE-STATE POWER FORECAST MODEL

Aggregated state m	1	2	3
Probability $\widetilde{pr}_{A,m}$	0.1875	0.6250	0.1875
Power output $\widetilde{P}_{A,m}$ (kW)	58.33	70	81.67

TABLE IV
EXAMPLE B: THREE HOURS OF AGGREGATED THREE-STATE POWER FORECAST MODEL

Aggregated state m	1	2	3
Probability $\widetilde{pr}_{A,m}$	0.1875	0.6250	0.1875
Power $\widetilde{P}_{A,m}$ (kW) at t = 1 h	58.33	70	81.67
Power $\widetilde{P}_{A,m}$ (kW) at t = 2 h	92.67	110	127.33
Power $\widetilde{P}_{A,m}$ (kW) at t = 3 h	29.17	35	40.83

the BESS for operation of the urban microgrid. An example on how to use the aggregated three-state power forecast model to determine hourly positive and negative energy reserves in the BESS is provided in the following.

B. Energy Reserve Assessment for Operation of Microgrid

International Journal of Research
Available at https://edupediapublications.org/journals
p-ISSN: 2348-6848
e-ISSN: 2348-795X
Volume 02 Issue 11
November 2015

Taking into account the aggregated wind and solar power forecast model developed above, an illustrative example is provided to show how the energy reserve is assessed. In Table IV, an aggregated three-state power forecast model for three continuous hours is assumed. The aggregated power forecast for hour 1 is taken from the example solved in Section III-A. The aggregated power forecast of hours 2 and 3 is calculated by the same method. As shown in Table IV, the probability of having real-time power output at state 1 in three continuous hours is equal to the product of the probabilities in state 1 for those three hours. This probability is thus equal to 0.18753=0.00659. This is also the same probability for having state 3 in three continuous hours. The probability is very small. Therefore, the BESS has enough negative energy reserve to cover for uncertainty for three successive hours if the following condition is met:

$$EC_{\text{NR-3h}} = (81.67 - 70)\ \text{kWh} + (127.33 - 110)\ \text{kWh} + (40.83 - 35)\ \text{kWh} = 34.83\ \text{kWh}.$$

Figure 5 battery storage capacity allocation for optimized scheduling

Power at aggregated state 3 represents the power forecast higher than average, state 2. Therefore, the negative reserve that is used to capture excess energy is calculated by summation of the energy pertaining to state 3 minus the energy pertaining to state 2 in a 3-h window. This means that the microgrid has, at the high probability of 1−0.18753 , the free capacity in the BESS to capture the excess of renewable energy for a 3-h window. Similar to the negative energy reserve assessment, the positive energy reserve is assessed. In order to calculate the positive energy reserve for the example shown in Table IV, energy of state 2 is subtracted from energy of state 1 for all three hours, and the results are summed up. Positive energy reserve is the stored energy in the BESS ready to be injected into the dc bus to mitigate less renewable power generation than expected

$$EC_{\text{PR-3h}} = (70 - 58.33)\ \text{kWh} + (110 - 92.67)\ \text{kWh} + (35 - 29.17)\ \text{kWh} = 34.83\ \text{kWh}.$$

Similar to the example solved for 1 h in Table III, the aggregated model should be developed for the whole dispatch period. For instance, if the scheduling horizon is 24 h, a window sweeps the horizon in 24/3 blocks. Thus, eight blocks of reserve will be determined. Both positive and negative energy reserves are considered in the BESS energy constraint. Based on the operation strategy, BESS storage capacity allocation is shown in Fig. 6. The depth of discharge (DOD), positive energy reserve (PR), operational area, and negative energy reserve (NR) are allocated in the BESS. The BESS can only be charged and discharged in the operation area in normal operation mode, which is scheduled by optimization. The BESS may operate in positive and negative energy reserve areas in order to compensate the uncertainties of power generation and load demand in realtime operation.

C. Formulation of Optimized Scheduling of Microgrid

The objective of the optimization is to minimize operation cost of the microgrid in interconnected mode and provide UPS service in the autonomous mode. These objectives can be achieved by minimization of the following defined objective function:

$$F(P_{\text{G}}, P_{\text{EVS}}) = \sum_{i=1\ \text{h}}^{T} C_{1\text{kWh}}(i) \times P_{\text{G}}(i) \times \tau_{\text{h}} + \sum_{i=1\ \text{h}}^{T} C_{1\text{kWh}}(i) \times P_{\text{EVS}}(i) \times \tau_{\text{h}} + \sum_{i=1\ \text{h}}^{T} EPBF \times \overline{EMS} \times P_{\text{G}}(i) \times \tau_{\text{h}} \quad (3)$$

Where F is the objective function to be minimized, Tis the scheduling horizon of the optimization,τh is the optimization time step which is 1 h, C1kWh is the energy cost for 1 kWh energy,PGis the incoming power from the grid, PEVSis the smart charging power for EVs,EPBFis the emission

International Journal of Research
Available at https://edupediapublications.org/journals
p-ISSN: 2348-6848
e-ISSN: 2348-795X
Volume 02 Issue 11
November 2015

penalty– bonus factor for CO2,andEMSis the average CO2 emission of 1 kWh electrical energy in the power system outside the microgrid. In this objective function,PGand PEVSare to be determined by optimization. The first term in the objective function above expresses the energy cost, the second term defines the cost of EV smart charging, and the third term describes the emission cost. As shown in Fig. 1, for positive values ofPG, the microgrid draws power from the main grid, and for negative values of PGthe microgrid injects power into the main grid. The emission term penalizes power flow from the main grid to the microgrid. If the microgrid draws power from the main grid, the microgrid would contribute to emissions of the power system. On the other hand, as the microgrid has no unit that produces emission, when the microgrid returns power to the main grid, it contributes to emission reduction. The optimization program determines a solution that minimizes the operation cost of the dc microgrid. Thus, a monetary value is assigned to emission reduction by this approach. This objective function is subject to the constraints as follows.

1) Power limitation of the grid interface introduces a boundary constraint to the optimization

$$P_{G-} \le P_G(t) \le P_{G+} \quad \forall t \in T \qquad (4)$$

wherePG−is the lower boundary of the grid power, and PG+is the upper boundary of the grid power.

2) The BESS power has to be within the limits

$$P_{BESS-} \le P_{BESS}(t) \le P_{BESS+} \quad \forall t \in T \qquad (5)$$

wherePBESS−is the lower boundary of the outgoing power from the BESS to the dc bus,PBESSis the BESS power to the dc bus, andPBESS+is the upper boundary of the BESS power.

3) The availability of EV and charging power limits should be met

$$0 \le P_{EVS}(t) \le P_{EVS+} \quad \forall t \in T_{EVS} \qquad (6)$$

Where PEVS is the EV charging power, PEVS+is the upper boundary of the EV charging power, andTEVS gives the hours in which EVs are available for smart charging. 4) The power balance equation has to be valid at all simulation time steps

$$\tilde{P}_{A,2}(t) + P_{BESS}(t) + P_G(t) - \tilde{P}_{EVF}(t) - P_{EVS}(t) = 0 \quad \forall t \in T \qquad (7)$$

wherePA,2 is the average power forecast of renewable energy sources wind and solar at aggregated state 2, and PEVFis the EV fast charging power forecast.

5) The objective function is also subject to a constraint of the SOC of the BESS. In order to include UPS service, the formulation of the optimization is modified. The key application is supplying loads by the microgrid for a defined time span in the case of a contingency. It is devised so that the microgrid provides backup power fora commercial load such as a bank branch or an officduring working hours. According to the system layout shown in Fig. 1, this constraint can be defined as follows:

$$E_{BESS-}(t) \le E_{BESS-0} - \sum_{j=1\,min}^{t} \Delta E_{BESS}(j) \le E_{BESS+}(t) \quad \forall t \in T \qquad (8)$$

Where EBESS−is the lower boundary of energy capacity of the BESS,EBESS-0 is the SOC of the BESS at the beginning of the optimization,EBESSis the discharged energy from the BESS to the dc bus at every minute, and EBESS+is the upper boundary of energy capacity of the BESS. The SOC of the battery at all time steps should be in the operation zone of the BESS. Therefore, in this equation, the SOC of the battery is calculated and checked to be within the upper and lower SOC limits. QuantitiesEBESS−, EBESS+,andEBESSare calculated as follows:

$$E_{BESS-}(t) = EC_{BESS} \times (1 - DOD) + EC_{PR\text{-}3h}(t) + EC_{UPS}(t) + \widetilde{EC}_{EVF}(t) \quad \forall t \in T \qquad (9)$$

International Journal of Research
Available at https://edupediapublications.org/journals
p-ISSN: 2348-6848
e-ISSN: 2348-795X
Volume 02 Issue 11
November 2015

Where EBESS−is the lower boundary of BESS SOC, ECBESSis the energy capacity of the BESS, DODis the depth of discharge of the BESS,ECPR-3his the positive energy reserve of the BESS to cover power forecast uncertainty,ECUPSis the energy capacity allocated in the BESS for the UPS service of the loads, andECEVFis the energy capacity forecast for fast charging demand. The first term in the equation takes into account the possible depth of discharge. The BESS cannot be charged up to the full capacity because negative energy reserve is scheduled in the BESS to capture potential excess renewable power as calculated in Section III-B. This boundary constraint is expressed by

$$E_{\mathrm{BESS+}}(t) = EC_{\mathrm{BESS}} - EC_{\mathrm{NR\text{-}3h}}(t) \quad \forall t \in T \quad (10)$$

Where EBESS+is the upper boundary of BESS SOC, ECBESS is the energy capacity of the BESS, and ECNR-3h is the negative energy reserve of the BESS. The discharged energy from the BESS to the dc bus is calculated by

$$\Delta E_{\mathrm{BESS}}(t) = \begin{cases} \frac{P_{\mathrm{BESS}}(t)}{\eta_{\mathrm{dis}}} \times \tau_{\min}, & P_{\mathrm{BESS}} \geq 0 \\ P_{\mathrm{BESS}}(t) \times \eta_{\mathrm{ch}} \times \tau_{\min}, & P_{\mathrm{BESS}} < 0 \end{cases} \quad (11)$$

Where EBESS is the discharged energy from the BESS to the dc bus in every minute, ηdis is the discharging efficiency of the BESS,ηch is the charging efficiency of the BESS, and τminis the time step size equal to 1 min.

6) The total required EV smart charging energy for the day-ahead scheduling is to be met. This is defined by an equality constraint

$$\sum_{i=1\,\mathrm{h}}^{T_{\mathrm{EVS}}} P_{\mathrm{EVS}}(i) \times \tau_{\mathrm{h}} = \widetilde{EC}_{\mathrm{EVS\text{-}ch}} \quad (12)$$

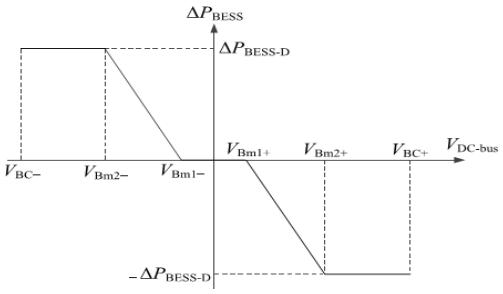

Figure 6 droop controlof BESS power electronic converter to mitigate power deviation of dc microgrid in normal SOC of the BESS

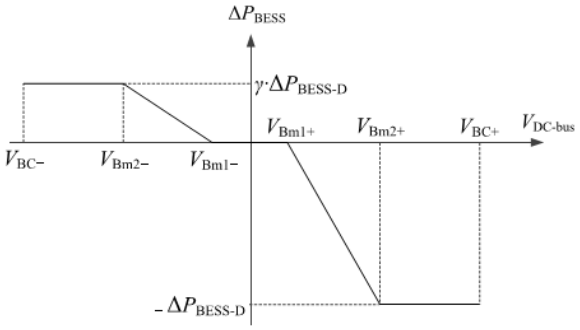

Figure 7 droop controlof BESS power electronic converter to mitigate power deviation of dc microgrid in lower than the scheduled SOC of the BESS

Where TEVS is the time that EVs are available for smart charging by the microgrid,PEVSis the smart charging power of EVs, and ECEVS-ch is the total EV smart charging energy forecast for the day-ahead scheduling

IV.ADAPTIVE DROOPCONTROL OF BESS .

In this section, the real-time operation of the microgrid in the interconnected and autonomous modes is studied. In the interconnected mode of operation, an adaptive droop control is devised for the BESS. The adaptive droop characteristic of the BESS power electronic converter is selected on the basis of the deviation between the optimized and real-time SOC of the BESS, as calculated in Section III. Details of the method are provided in Section IV-A. In autonomous mode of operation, the BESS is responsible for keeping the voltage of the dc bus in a defined acceptable range for providing UPS service. The autonomous mode of

International Journal of Research
Available at https://edupediapublications.org/journals
p-ISSN: 2348-6848
e-ISSN: 2348-795X
Volume 02 Issue 11
November 2015

operation of the microgrid is described in Section IV-B.

A. DC Voltage Droop Control in Interconnected Mode

The devised droop controls of the BESS are depicted in Figs. 7–9. The change of the battery power PBESS is

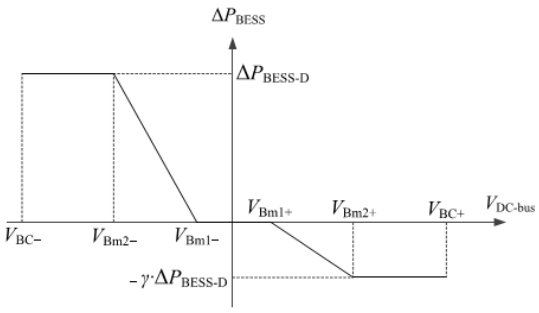

Figure 8 Figure 7 droop controlof BESS power electronic converter to mitigate power deviation of dc microgrid in higher than the scheduled SOC of the BESS

modified as a function of the dc voltage. It can be noted that two of the three devised droop characteristics are asymmetric. The first droop curve, as shown in Fig. 7, is devised for a case where the real-time SOC of the BESS is within close range of the optimized SOC of the BESS from the scheduling calculated in Section III-C. The acceptable realtime SOC is determined throughdefinition of upper and lower boundaries around the optimized SOC. If the real-time SOC is within these boundaries, the droop control of the BESS power electronic converter is selected as shown in Fig. 7 to support the dc voltage. In this case, the upper boundary and the lower boundary lead to a symmetrical droop response. In the voltage range between VBm1−andVBm1+, battery storage does not react to the voltage deviations of the dc bus. In the voltage range fromVBm1−to VBm2−and also from VBm1+ to VBm2+, the droop control of the BESS reacts. Therefore, PBESS modifies the power outputPBESS to mitigate the voltage deviation of the dc bus. Finally, in the voltage range fromVBm2−to VBC−and also fromVBm2+to VBC+, the droop curve is in a saturation area, and thus the BESS contribution is at its maximum and constant. The second droop curve as shown in Fig. 8 is devised for a situation where the real-time SOC of the BESS is lower than the optimized and scheduled SOC of the BESS. Therefore, the BESS contributes to stabilizing the dc bus voltage by charging at the same power as shown in Fig. 7. However, the upper boundary of the BESS droop response is reduced by the factorγ, and it is equal to γ·PBESS-D. This way, the SOC can come closer to the optimized and scheduled SOC. The third droop curve as shown in Fig. 9 is devised for a situation where the real-time SOC of the BESS is higher than the optimized and scheduled SOC of the BESS. Therefore, the BESS contributes to stabilizing the dc bus voltage by discharging at the same power as shown in Fig. 7. However, the lower boundary of the BESS droop response is modified by the factorγ, and it is equal to −γ·PBESS-D. The dc–ac converter connected to the main grid is also controlled by a droop, as shown in Fig. 10. The droop parameters are adjusted to support the droop control of the storage. The boundaries must respect the capacity of the converter. In real-time operation and interconnected mode, the SOC of the BESS is measured and compared against the optimized SOC of the BESS, and the proper droop will be selected as

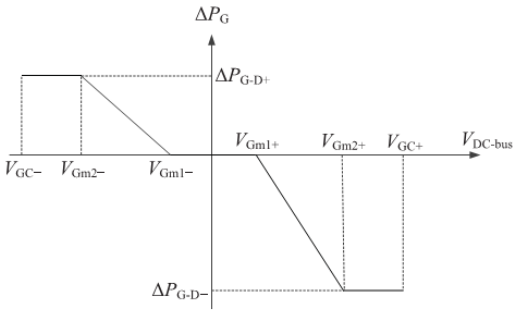

Figure 9 Figure 7 droop control of grid power electronic converter interconnected operation mode of dc microgrid

International Journal of Research
Available at https://edupediapublications.org/journals
p-ISSN: 2348-6848
e-ISSN: 2348-795X
Volume 02 Issue 11
November 2015

TABLE V

ADAPTIVE DROOP SELECTION FOR THE BESS

SOC of the BESS in real-time	Droop curve
Close to the optimized scheduling	BESS droop 1 (Fig. 7)
Lower than in optimized scheduling	BESS droop 2 (Fig. 8)
Higher than in optimized scheduling	BESS droop 3 (Fig. 9)

described above. A summary of the droop selection for the BESS in interconnected operation mode is shown in Table V.

B. DC Voltage Droop Control in Autonomous Mode

In the autonomous mode, the main grid is disconnected. Then, the fast charging service has less priority compared with the supply of other loads. The control of the BESS converter is also defined by the voltage–power droop as discussed. The BESS so supports the voltage of the dc bus.

V. VERIFICATION BYSIMULATION

The proposed operational method of the urban microgrid in day-ahead scheduling and real-time operation is verified by simulation. For the day-ahead scheduling, the method introduced in this paper is implemented in MATLAB and simulated for a case study.

A. Simulation of Optimized Scheduling

The optimized scheduling of a vertically integrated urban microgrid with renewable energy harvesting as shown in Fig. 2 and EV charging on the ground is verified for the following assumptions.

1) A vertical axis wind turbine with a generation capacity of 100 kW is installed on the rooftop.

2) Photovoltaic panels with a generation capacity of 50 kW are mounted on the building.

3) A flow battery with the energy capacity of 1000 kWh, power rating of 400 kW, and charging and discharging efficiencies of 0.95 and 0.90, respectively, is placed inthe basement of the building. The SOC of the BESS at the beginning of the optimization is assumed to

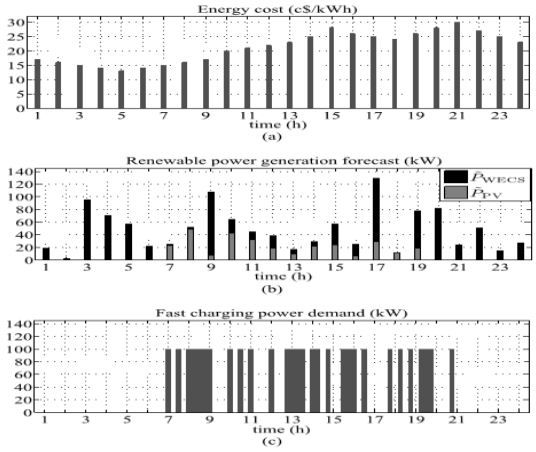

Case study: Inputs. (a) 1 kWh energy cost profile. (b) Average wind and solar power forecast profiles. (c) Fast charging profile of electric vehicles.

be 300 kWh. TheDODof the BESS is 80% of the maximum energy capacity, which gives a minimum possible discharge to SOC of 200 kWh.

4) A supercapacitor storage with a capacity of 100 kW is installed.

5) The BESS and supercapacitor together form a multilevel energy storage, where the supercapacitor provides fast dynamic response under an energy cache control scheme [19].

6) The dc bus capacitance is distributed among converters according to rating and in sum is 40 mF.

7) A grid interface with the capacity of 300 kW is provided.

8) The energy cost diagram for 1 kWh energy is given in Fig. 11(a).

9) The power generation forecast curves of the wind and PV-based power generation are shown in Fig. 11(b).

10) A fast charging station to serve one EV at a time is provided. The charging power is 100 kW. A uniform distribution function is employed to simulate the demand of fast charging in each quarter of an hour from 7AM to 9 PM. The simulated fast charging profile is provided in Fig. 11(c).

11) The average amount of CO2 emission to generate 1 kWh electricity in the power system

International Journal of Research
Available at https://edupediapublications.org/journals
p-ISSN: 2348-6848
e-ISSN: 2348-795X
Volume 02 Issue 11
November 2015

(EMS)is 0.61235 kg/kWh [21]. The emission penalty–bonus

TABLE VI
CASE STUDY: ASSUMED INDIVIDUAL WIND AND SOLAR POWER FORECAST UNCERTAINTY DATA

Individual state	State 1	State 2	State 3
Wind forecast probability	0.25	0.50	0.25
Wind power forecast error (%)	-20%	0%	+20%
Solar forecast probability	0.25	0.50	0.25
Solar power forecast error (%)	-25%	0%	+25%

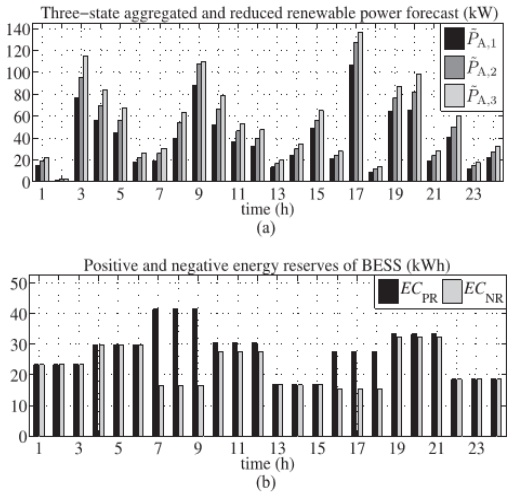

Fig. 12. Case study: Three-state aggregated renewable power generation model and reserve allocation. (a) Three-state aggregated wind and solar power forecast profile. (b) Positive and negative energy reserve profiles of BESS.

factor (EPBF)of3c$/kgCO2 is chosen for the optimization.

12) The UPS service is devised for 50 kW power and 4 h of continuous supply from 8AMto 4 PM.

13) EVs are available for smart charging from 8PMto the next day at 7AM. The maximum smart charging power of the aggregated EVs is 20 kW. The daily demand of EVs is forecasted to be 50 kWh.

Based on the method to aggregate uncertainty of forecast of the renewable resources formulated in Section III-A, the wind and PV power are aggregated. In order to generate the aggregated three-state model for the renewable resources of the urban microgrid, forecast uncertainties are assumed as shown in Table VI. In this table, wind and solar power forecast error data are provided in percentage power deviations from the average value in state 2. These data apply to the wind and solar power profiles as shown in Fig. 11(b). From the aggregated three-state model shown in Fig. 12(a), based on the method introduced in Section III-A, the 3-h window of positive and negative energy reserves in the BESS is determined as depicted in Fig. 12(b) and explained in Section III-B. As shown, in each 3-h window starting at hour 1, the positive and negative energy reserves are often the same. It can happen that the positive and negative reserves are not equal. This has happened twice for windows covering hours 7 to 9 and 16 to 18. At hours 9 and 17, wind power as

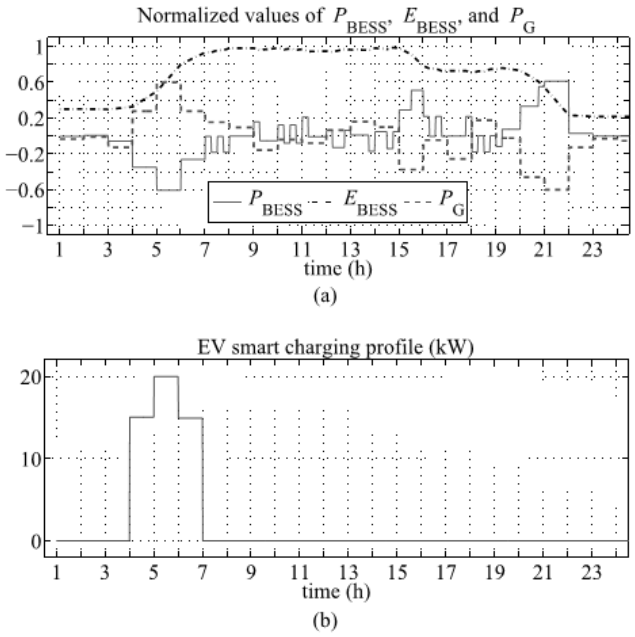

Fig. 13. Case study: Cost-optimized scheduling of dc microgrid. (a) Optimized scheduling results of the BESS and the grid. BESS and grid power profiles are in per unit of 500 kW, and BESS energy profile is in per unit of 1000 kWh. (b) Optimized charging profile of EVs

.

shown in Fig. 11(b) is at the maximum. Based on the power rating of the wind turbine, at those hours the output power cannot exceed the nominal value. Asa result, the wind power of state 2 is equal to the maximum value of power as in state 3. Consequently, less negative reserve is required

International Journal of Research
Available at https://edupediapublications.org/journals
p-ISSN: 2348-6848
e-ISSN: 2348-795X
Volume 02 Issue 11
November 2015

since the wind power in state 3 is equal to wind power in state 2. The optimization method is implemented in the MATLAB Optimization Toolbox. The active-set algorithm is used to solve the optimization problem with the linear objective function and the associated constraints. Power limits of the components are translated into power boundary conditions in the implemented optimization code. The power balance constraint (7) is implemented as equality constraint.

The total required smart EV charging energy (12) is also implemented as an equality constraint. The BESS energy constraint (8) is implemented by an array of inequality constraints. Simulation results are provided in Fig. 13(a) and (b). The battery power delivered to the dc bus of the urban microgrid, SOC of the battery, and power coming from the main grid are given. As shown, the BESS is charged when the energy price is relatively low. The urban microgrid injects power to the grid at high energy prices. The urban microgrid is able to supply all the fast charging demand. From 8AMto 4 PM,the urban microgrid has adequate SOC to provide 50 kW UPS for a duration of four continuous hours. Thanks to the optimized operation strategy, all the objectives of the urban microgrid operation are met.

B. Simulation of Adaptive DC Voltage Droop Control

The layout of the urban microgrid which is implemented in PSCAD [20] is shown in Fig. 1. The power electronic

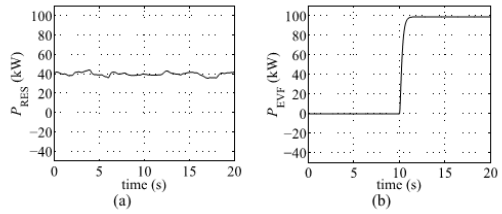

Fig. 14. Case study: Assumptions of the simulation. (a) Renewable power generation. (b) Fast charging load connected to the dc bus.

converters are represented as average models [22], [23]. The voltage–power droop control that is described in Section IV for real-time operation of the urban microgrid is implemented. In this subsection, 20 s around the time 12:45 PMin the optimized scheduling of Section V-A are considered. At this time, the BESS charges at 70 kW, power drawn from the grid is 32 kW, and the average renewable power is 38 kW. Renewable power generation is simulated for 20 s as shown in Fig. 14(a). The fast charging load is connected to the dc bus at time equal to 10 s at 100 kW as shown in Fig. 14(b). For droop control of the BESS converter in normal SOC of the BESS in Fig. 7, the following assumptions are made:VBm1 =(380±1) V,VBm2 =(380±6) V, a n PBESS-D=200 kW. The BESS converter droop is set to react on voltage deviations higher than 1 V, and deviations below that value are neglected. The BESS converter power reaches its maximum change at dc bus voltage deviations of 6 V and higher. The main grid converter droop settings are assumed as follows: VGm1 =(380±5) V,VGm2 =(380±10) V, and maximum grid power is 300 kW. The voltage margins for the droop control of the grid converter are coordinated with the voltage margins for the droop control of the BESS converter in order to achieve the priority of BESS participation in controlling the voltage of the dc bus. Alternative approaches for coordinated droop controls of the converters may be found depending on the objective of the operation. In case A, it is assumed that the SOC of the battery is within close range of the scheduled SOC resulting from the day-ahead optimization. Therefore, the droop control in normal SOC of the battery as depicted in Fig. 7 is employed. The simulation results are shown in Figs. 15–17. The powerPMESdelivered by the multilevel energy storage combination of BESS and supercapacitor compensates both fast changes of renewable fluctuations and load. The rapid decrease of−PMESat 10 s shows that power is made readily available for fast charging. Thanks to the supercapacitor as cache energy storage, the power fluctuations do not propagate to the main grid. The grid power to the dc bus is unchanged. The droop control of the main grid converter is not active, and thus the grid power remains the same as scheduled. The functionality of the BESS droop control can be recognized from Fig. 16. The dc bus voltage dropped approximately by 2.6 V and

International Journal of Research
Available at https://edupediapublications.org/journals
p-ISSN: 2348-6848
e-ISSN: 2348-795X
Volume 02 Issue 11
November 2015

stabilized around 376.4 V as seen in Fig. 17. In case B, it is assumed that the BESS has lower than expected SOC compared with the SOC scheduled in the

Fig. 15. Case A: Droop-control-based responses to wind fluctuation and fast charging when SOC of battery is as scheduled.

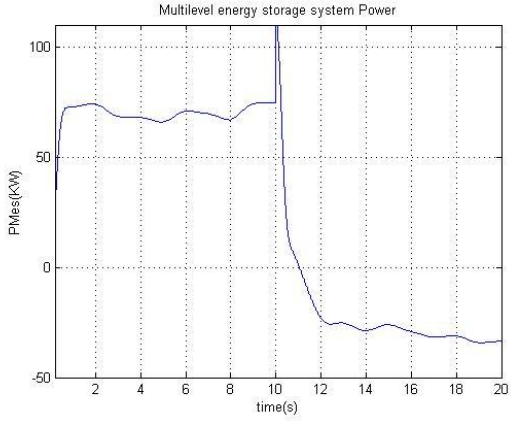

(a) Multilevel energy storage system (MES) charging power from the dc bus.

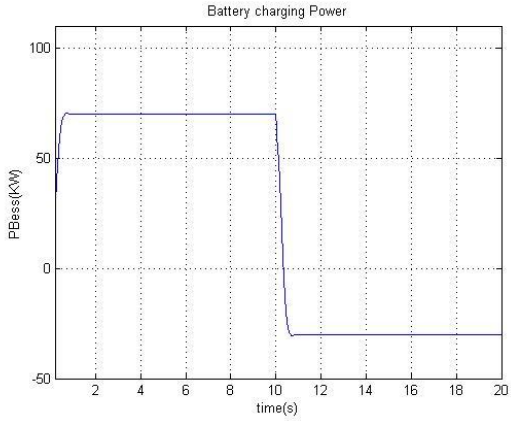

(b) Battery charging power from the dc bus.

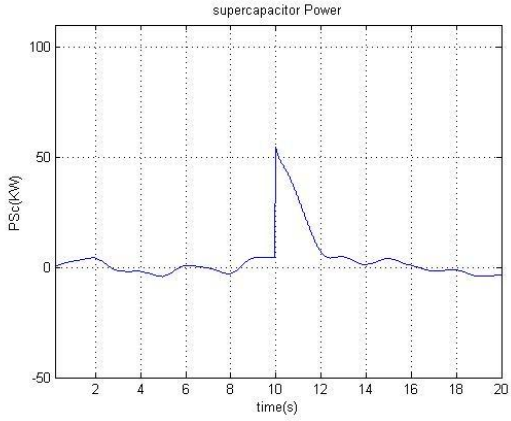

(c) Supercapacitor discharging power to the dc bus.

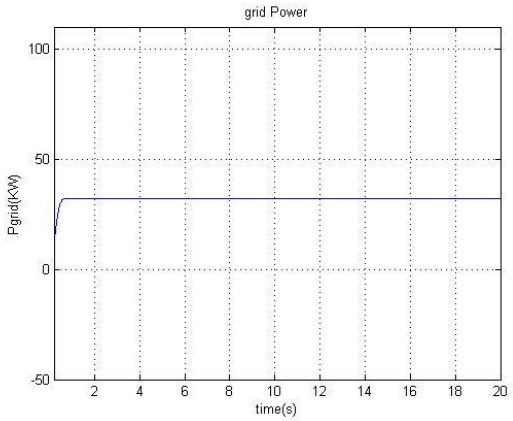

(d) Grid power to the dc bus.

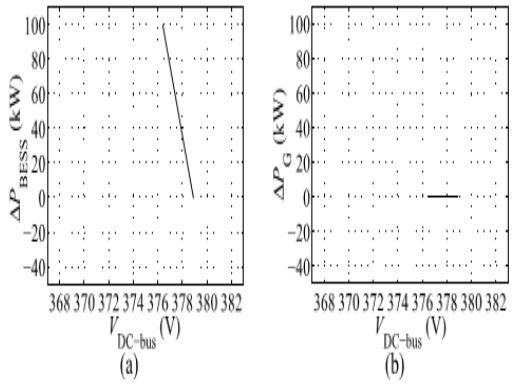

Fig. 16. Case A: BESS and grid droop response curves. (a) Droop response curve of BESS. (b) Droop response curve of grid.

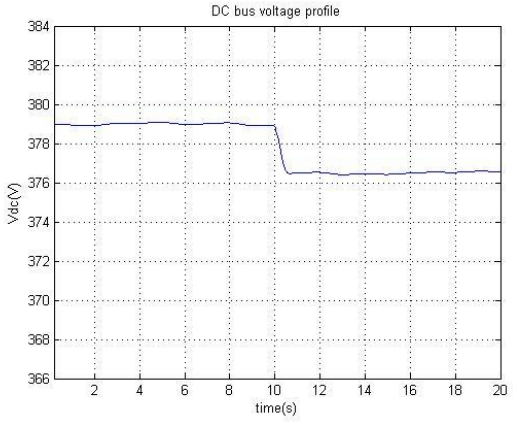

Fig. 17. Case A: dc bus voltage profile.

optimization. As a result, the BESS droop control as depicted in Fig. 8 is selected. In the new droop control, γis 0.33. All other assumptions are the

International Journal of Research
Available at https://edupediapublications.org/journals
p-ISSN: 2348-6848
e-ISSN: 2348-795X
Volume 02 Issue 11
November 2015

same as in case A where the fast charging load is connected to the dc bus at time 10 s. The simulation results are depicted in Figs. 18–20. With the asymmetric droop curve of the BESS of Fig. 8, the multilevel energy storage in case B does not provide full compensation of renewable fluctuations and the heavy fast charging EV. So, the droop control of the grid is also activated, and the main grid contributes to the fast charging power demand. The BESS power is without fluctuation thanks to the

Fig. 18. Case B: Droop-control-based responses to wind fluctuation and fast charging when SOC of battery is lower than scheduled

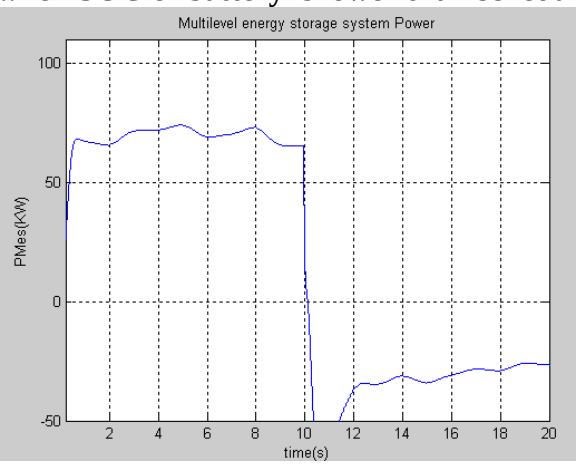

. (a) Multilevel energy storage system (MES) charging power from the dc bus.

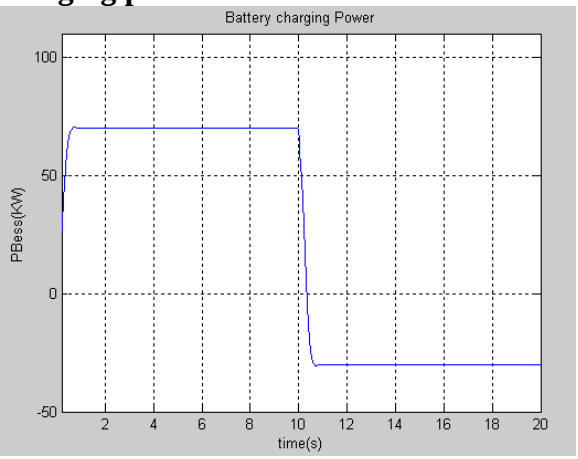

(b) Battery charging power from the dc bus.

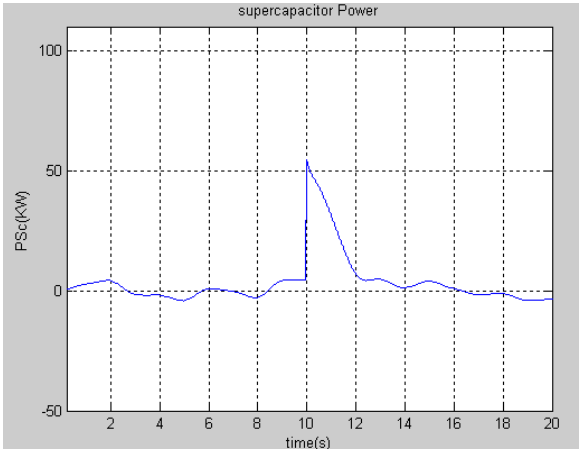

(c) Supercapacitor discharging power to the dc bus

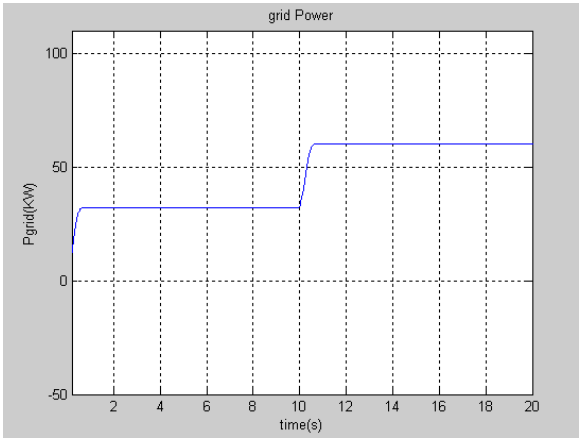

. (d) Grid power to the dc bus.

Fig. 19. Case B: BESS

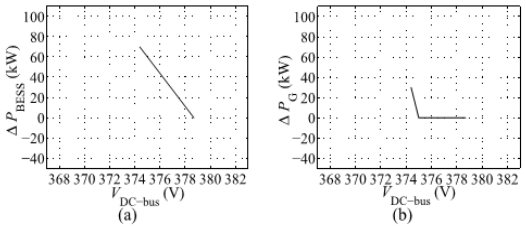

and grid droop response curves. (a) Droop response curve of BESS. (b) Droop response curve of grid.

International Journal of Research
Available at https://edupediapublications.org/journals
p-ISSN: 2348-6848
e-ISSN: 2348-795X
Volume 02 Issue 11
November 2015

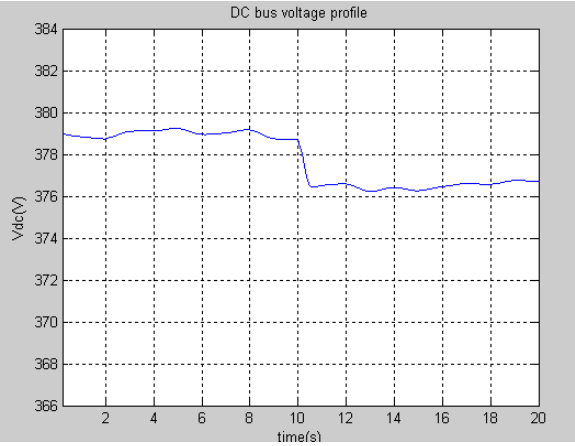

Fig. 20. Case B: dc bus voltage profile.

supercapacitor, which absorbs the rapid power fluctuations. The dc bus voltage drops to around 374.4 V as shown in Fig. 20. The voltage drop is higher than in case A. This is due to the wider range of droop control characteristics of the main grid converter and less contribution of the BESS to voltage control. The functionality of the BESS and grid droop control can be recognized from Fig. 19. The comparison of the results shows the importance of coordinating the droop settings with the scheduling in microgrids with wind and solar power. While in Fig. 15 the SOC of the battery is as desired according to the scheduling, the SOC of the battery has become lower than expected due to forecast uncertainty in Fig. 18. In the latter case, the asymmetric droop of Fig. 8 avoids further significant discharging, but has full droop contribution on the charging side. On the reduced discharging side, the droop of the other power electronic converter connecting to the main grid kicks in to keep up the dc voltage if necessary. From Fig. 19, it can be seen that the droop response of the grid converter becomes active at VDC-bus =375 V. Above that level, the droop control of the converter connected to the storage acts on its own. As it does so at a lower response compared with the case where the SOC is not below the scheduled level, the steady-state ripple of VDC-bus in the first 10 s is higher in Fig. 20 than it is in Fig. 17.

VI. CONCLUSION

A dc microgrid for renewable power integration has been proposed. The operational optimization and power-electronicsbased voltage–power droop control was developed, and the functioning was demonstrated through simulation. Interaction with the main grid was controlled as a result of an operational optimization that seeks to minimize cost and emissions. A method to quantify the uncertainty affiliated with the forecast of aggregated wind and PV-based power generation was created and used to quantify the energy reserve of the battery energy storage system. The battery is parallel-connected with a supercapacitor to form a multilevel energy storage. The latter plays a critical role in compensating renewable power fluctuations and providing the power needed when EVs stop by for fast charging. In accordance with the microgrid paradigm, operation is also supported in autonomous mode to support UPS when the connection to the main grid is unavailable. During such periods, fast charging is not supported, as the priority shifts to supplying critical local loads. Power electronics is a key enabling technology in connecting all energy resources to the dc bus. The converters support the dc voltage through a droop control scheme. The control proposed here is adaptive in that the voltage–power droop curves are modified depending on the outcome of the operational optimization. As a novelty, asymmetric droop curves were proposed for the converters connected to the storage so as to also support the objective of bringing the actual battery SOC close to the desired one as scheduled. This ensures, in particular for the multilevel energy storage, that the contribution toward dc voltage control does not compromise its role in providing adequate energy reserve. For the special case of an urban location, the vertical integration within a tower building offers renewable wind and solar power harvesting on the top and energy delivery at the bottom on the ground level, for example for EV charging. The structure contributes to closely co-locating renewable power generation and delivery to local stationary and mobile EV energy resources. In sum, this paper contributes to the microgrid

paradigm by a novel droop control that takes into account storage SOC when adaptively setting the slopes of the voltage–power droop curves; the proposed forecast based on aggregation of renewable power generation contributes to quantifying energy reserve. In an urban setting, a tower-integrated installation to co-locate harvesting of wind energy and local delivery of clean energy is an alternative. The optimization for power exchanges and dc voltage control using adaptive control are performed through power electronic converters that serve as interfaces to all resources. The resulting energy system serves local stationary and EV-based mobile consumers, and it is a good citizen within the main grid as it reduces emissions by local usage of wind and solar energy.

REFERENCES

[1]"Global Wind Report: Annual Market Update 2012."Global Wind Energy Council Brussels, Belgium Tech.Rep.,2012

[1] "Globalwind report: Annual market update 2012," Global Wind Energy Council, Brussels, Belgium, Tech. Rep., 2012.

[2] H. Polinder, J. A. Ferreira, B. B. Jensen, A. B. Abrahamsen, K. Atallah, and R. A. McMahon, "Trends in wind turbine generator systems,"IEEE J. Emerg. Sel. Topics Power Electron., vol. 1, no. 3, pp. 174–185, Sep. 2013.

[3] F. Giraud and Z. M. Salameh, "Steady-state performance of a gridconnected rooftop hybrid wind-photovoltaic power system with battery storage," IEEE Trans. Energy Convers., vol. 16, no. 1, pp. 1–7, Mar. 2001.

[4] B. S. Borowy and Z. M. Salameh, "Methodology for optimally sizing the combination of a battery bank and PV array in a wind/PV hybrid system," IEEE Trans. Energy Convers., vol. 11, no. 2, pp. 367–375, Mar. 1996.

[5] M. Cheng, S. Kato, H. Sumitani, and R. Shimada, "Flywheel-based AC cache power for stand-alone power systems,"IEEJ Trans. Electr. Electron. Eng., vol. 8, no. 3, pp. 290–296, May 2013.

[6] H. Louie and K. Strunz, "Superconducting magnetic energy storage (SMES) for energy cache control in modular distributed hydrogenelectric energy systems,"IEEE Trans. Appl. Supercond., vol. 17, no. 2, pp. 2361–2364, Jun. 2007.

[7] A. L. Dimeas and N. D. Hatziargyriou, "Operation of a multiagent system for microgrid control,"IEEE Trans. Power Syst., vol. 20, no. 3, pp. 1447–1455, Aug. 2005.

[8] F. Katiraei and M. R. Iravani, "Power management strategies for a microgrid with multiple distributed generation units," IEEE Trans. Power Syst., vol. 21, no. 4, pp. 1821–1831, Nov. 2006.

[9] A. G. Madureira and J. A. Pecas Lopes, "Coordinated voltage support in distribution networks with distributed generation and microgrids,"IET Renew. Power Generat., vol. 3, no. 4, pp. 439–454, Dec. 2009.

[10] M. H. Nehrir, C. Wang, K. Strunz, H. Aki, R. Ramakumar, J. Bing, et al., "A review of hybrid renewable/alternative energy systems for electric power generation: Configurations, control, and applications," IEEE Trans. Sustain. Energy, vol. 2, no. 4, pp. 392–403, Oct. 2011.

[11] R. Majumder, B. Chaudhuri, A. Ghosh, R. Majumder, G. Ledwich, and F. Zare, "Improvement of stability and load sharing in an autonomous microgrid using supplementary droop control loop,"IEEE Trans. Power Syst., vol. 25, no. 2, pp. 796–808, May 2010.

[12] D. Westermann, S. Nicolai, and P. Bretschneider, "Energy management for distribution networks with storage systems—A hierarchical approach," inProc. IEEE PES General Meeting, Convers. Del. Electr. Energy 21st Century, Pittsburgh, PA, USA, Jul. 2008.

[13] A. Chaouachi, R. M. Kamel, R. Andoulsi, and K. Nagasaka, "Multiobjective intelligent energy management for a microgrid,"IEEE Trans. Ind. Electron., vol. 60, no. 4, pp. 1688–1699, Apr. 2013.

[14] R. Palma-Behnke, C. Benavides, F. Lanas, B. Severino, L. Reyes, J. Llanos, et al., "A microgrid energy management system based on the rolling horizon strategy," IEEE Trans. Smart Grid, vol. 4, no. 2, pp. 996–1006, Jun. 2013.

[15] R. Dai and M. Mesbahi, "Optimal power generation and load management for off-grid hybrid power systems with renewable sources via mixed-integer programming," Energy Convers. Manag., vol. 73, pp. 234–244, Sep. 2013.

[16] H. Kakigano, Y. Miura, and T. Ise, "Low-voltage bipolar-type DC microgrid for super high quality distribution,"IEEE Trans. Power Electron., vol. 25, no. 12, pp. 3066–3075, Dec. 2010.

[17] D. Chen, L. Xu, and L. Yao, "DC voltage variation based autonomous control of DC microgrids," IEEE Trans. Power Del., vol. 28, no. 2, pp. 637–648, Apr. 2013.

[18] L. Roggia, L. Schuch, J. E. Baggio, C. Rech, and J. R. Pinheiro, "Integrated full-bridge-forward DC-DC converter for a residential microgrid application,"IEEE Trans. Power Electron., vol. 28, no. 4, pp. 1728–1740, Apr. 2013.

[19] K. Strunz and H. Louie, "Cache energy control for storage: Power system integration and education based on analogies derived from computer engineering,"IEEE Trans. Power Syst., vol. 24, no. 1, pp. 12 19, Feb. 2009.

[20] "EMTDC transient analysis for PSCAD power system simulation version 4.2.0," Manitoba HVDC Research Centre, Winnipeg, MB, Canada, Tech. Rep., 2005.

[21] "Carbon dioxide emissions from the generation of electric power in the United States," Dept. Energy, Environmental Protection Agency, Washington, DC, USA, Tech. Rep., 2000.

[22] A. Yazdani and R. Iravani, Voltage-Sourced Converters in Power Systems. New York, NY, USA: Wiley, 2010.

[23] E. Tara, S. Filizadeh, J. Jatskevich, E. Dirks, A. Davoudi, M. Saeedifard, et al., "Dynamic average-value modeling of hybrid-electric vehicular power systems,"IEEE Trans. Power Del., vol. 27, no. 1, pp. 430–438, Jan. 2012.